Geochemical Perspectives Letters

Martian core composition from experimental high-pressure metal-silicate phase equilibria

H. Gendre[1*], J. Badro[1], N. Wehr[1], S. Borensztajn[1]

OPEN ACCESS

https://doi.org/10.7185/geochemlet.2216

Abstract

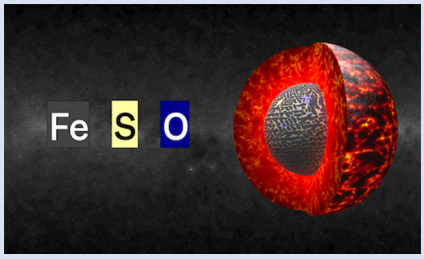

Current Martian core composition models suggest an iron-rich core alloyed with 10 to 20 wt. % of sulfur. Although Mars is more oxidised than Earth, oxygen is usually discarded as a potential light element candidate, since its dissolution into iron is negligible at the pressures and temperatures prevailing during Mars's primitive differentiation. However, it has recently been shown that oxygen interacts with the sulfur in the metal, which dramatically increases its solubility. Here, we investigated this novel process by carrying out metal-silicate equilibration experiments between 2 and 12 GPa, and 1673 and 2473 K, using piston-cylinder and multi-anvil presses. The experimental results show that oxygen was systematically incorporated in the metallic phase alongside sulfur, and a thermodynamic model was developed to parametrise this interaction. The oxygen-sulfur interaction parameter arising from those thermodynamic equations was fitted and used in a multi-stage core modelling simulation. We found that a Martian core containing 14 to 19 wt. % S (maximum permissible concentration according to cosmochemical constraints) will also contain between 1.3 and 3.5 wt. % O. This would help to match the Martian core density estimate while being cosmochemically consistent.

Received 1 February 2022 | Accepted 29 March 2022 | Published 11 May 2022

Introduction

Like the Earth, Mars's core is essentially made of Fe + Ni alloyed with lighter elements (S, O, Si, C, H). Although Mars's accretion and its bulk chemical composition are still uncertain (Bertka and Fei, 1998; Yoshizaki and McDonough, 2020), the composition of Martian meteorites (Dreibus and Wanke, 1985; McSween, 1994; Lodders and Fegley, 1997; Sanloup *et al.*, 1999; Taylor, 2013; Righter, 2017), the geophysical and geodetic data collected by spacecrafts and landers (Rivoldini *et al.*, 2011; Khan *et al.*, 2018; Stähler *et al.*, 2021) and high-pressure, high-temperature experimental work (Fei *et al.*, 1995; Morard *et al.*, 2007, 2018; Terasaki *et al.*, 2019) all argue for a sulfur-rich Martian core. This has led studies on Mars's core to focus on sulfur as an alloying element, with estimates ranging from 3.5 wt. % (Morgan and Anders, 1979) up to 36 wt. % S (Zharkov and Gudkova, 2005).

According to recent results on the elastic properties of Fe–Ni–S liquids, 30 wt. % S is required to fit the core density estimate (6000 ± 300 kg/m^3) if S is the only light element (Terasaki *et al.*, 2019; Stähler *et al.*, 2021). Paradoxically, such a high S-fraction exceeds the maximum sulfur concentration (~18–19 wt. %) that satisfies cosmochemical observables (Steenstra and van Westrenen, 2018; Brennan *et al.*, 2020). Alternatively, the dissolution of at least another light element can reduce the density to the current Martian estimate without impeding on those observables. For instance, Stähler *et al.* (2021) suggest 5 wt. % O in addition to 10 to 15 wt. % S to satisfy the density requirement, but they do not provide a mechanism to account for its dissolution in iron. Indeed, oxygen is known to be soluble in liquid iron only at high pressures and temperatures (Ohtani *et al.*, 1984; Ricolleau *et al.*, 2011; Siebert *et al.*, 2013; Badro *et al.*, 2015) which are not prevalent on smaller planets, such as Mars. Yet, another way to incorporate oxygen in the Martian core is through chemical interaction with sulfur in an Fe-liquid, that can drive its dissolution in the metal at lower pressures and temperatures (Tsuno *et al.*, 2011).

Here, we quantified the amount of oxygen that can be dissolved in the Martian core by taking into account oxygen-sulfur interaction. High-pressure, high-temperature metal-silicate equilibration experiments were carried out on Martian-like compositions and at Martian P and T conditions. The amount of S in the metal varied from 8 to 15 wt. %, and its effect on oxygen dissolution in the core was measured. Using thermodynamic modelling, we parametrised the oxygen-sulfur interaction from the experimental data and tested the robustness of the model to validate its predictive potential. We then applied our model to constrain the composition of the Martian core using multi-stage core formation modelling.

Methods

We conducted piston cylinder (PC) and multi-anvil press (MAP) experiments in MgO capsules between 2 and 12 GPa. The starting materials are made of an 18 wt. % FeO ultramafic silicate, representative of the Martian mantle, and an Fe–S metallic alloy, representative of the Martian core. Different sulfur fractions were

1. Université Paris Cité, Institut de Physique du Globe de Paris, CNRS, 75005 Paris, France
* Corresponding author (email: gendre@ipgp.fr)

tested, by varying the ratios of Fe and FeS in the metal, to cover a range of plausible sulfur concentrations going from 8 to 15 wt. %. The silicate and metal were then mixed, compressed, heated between 1673 and 2473 K, and equilibrated between 2 and 10 minutes. Textural observations and chemical analyses were conducted with a Zeiss Auriga 40 field emission scanning electron microscope equipped with a Bruker EDX spectrometer. Measurements were carried out using a focused beam raster and the resulting averages were obtained by statistical analyses of such scanned regions. We ensured that all the samples fully melted and reached equilibrium from their chemical homogeneity and texture that displays a large metallic blob in a silicate matrix (Fig. S-1). More details on the experimental procedure are provided in the supplementary material as well the detailed chemical composition of the starting materials (Tables S-1 and S-2) and recovered samples (Table S-3).

Results

As seen on the backscattered electron (BSE) image of a typical run (Fig. 1), the metallic phase systematically undergoes exsolution to iron-rich and sulfur-rich phases during quench, as previously reported (Blanchard *et al.*, 2015). It also includes a small fraction of oxide phases that show up as dark blobs in the brighter metal (Fig. 1b). These blobs are almost always located in the sulfur-rich zones (darker grey areas in Fig. 1b) which already suggests an affinity between S and O. This is confirmed by chemical analysis of the metal as plotted in Figure S-2 alongside similar data from Blanchard *et al.* (2015). The composition of the whole metallic phase was averaged to yield that of the homogeneous high-temperature melt, and we observe a positive correlation between the sulfur and oxygen concentrations, despite the fact that experiments were not performed at the same T and P.

Combining the data of Blanchard *et al.* (2015) with our dataset, we further parametrised the O-S interaction to evaluate the potential oxygen concentration in an S-rich Martian core. Starting from the dissolution reaction of oxygen into metal, $FeO^{silicate} = Fe^{metal} + O^{metal}$, we imposed the minimisation of the standard state Gibbs free energy of reaction $\Delta_r G°_{P,T}$ at thermodynamic equilibrium to obtain the expression that we fitted (the thermodynamic framework is detailed in the supplementary material):

$$\log\left(\frac{x_{Fe}\cdot x_O}{x_{FeO}}\right) = a + \frac{b}{T} + c\frac{P}{T} - \log(\gamma_{Fe}) - \log(\gamma_O) \quad \text{Eq. 1}$$

P, T and the x_i (i = O, Fe, FeO) respectively refer to the pressure, temperature and molar concentrations of O and Fe in the metal and FeO in the silicate. $\log(\gamma_{Fe})$ and $\log(\gamma_O)$ are the activity coefficients of Fe and O in the metallic melt, given in the supplementary material (Eqs. S-13 and S-14). They depend on the molar concentrations of the solutes (S and O) in the metal and on the interaction parameters between them (ε_O^S, ε_O^O and ε_S^S). P, T and the x_i (here i refers to O, S, Fe, FeO) are all known and the O-O and S-S interaction parameters were taken from Badro *et al.* (2015). The unknowns are a, b, c and ε_O^S, the thermodynamic interaction parameter between O and S in iron metal. The ε_O^S parameter describes how S affects the metal-silicate partitioning of O, a negative value meaning that the presence of S favours the presence of O in the metallic alloy, and therefore enhances its solubility, all other things being equal.

Using Equation 1, we performed a multivariate linear regression on the experimental data in order to estimate the thermodynamic parameters controlling oxygen dissolution in metal, *i.e.* a, b, c and ε_O^S. The first fit returned a c parameter that was statistically irrelevant ($c = -12 \pm 24$ K GPa^{-1} with an associated p-value of 0.63), showing no influence of pressure on the oxygen dissolution over the pressure range being considered (from 2 to 12 GPa). This pressure term was removed for the second fit ($R^2 > 0.97$) for which we obtained $a = 1.9 \pm 0.2$, $b = (-9.3 \pm 0.3) \times 10^3$ K and a negative value of -6.2 ± 0.6 for ε_O^S. The latter strongly deviates from the value of -17 found in the metallurgy literature (*Steelmaking Data Sourcebook*, 1988) determined at room pressure and that cannot reproduce the data well as seen on Figure S-4.

The robustness and predictive potential of our thermodynamic model was further investigated by calculating the expected oxygen concentration for each experimental run (*i.e.* for a given x_S, x_{Fe}, x_{FeO} and T) and comparing it to the measured value. Removing the pressure term in Equation 1 and rearranging the expression gives:

$$\log(x_O) = a + \frac{b}{T} + \log\left(\frac{x_{FeO}}{x_{Fe}}\right) - \log(\gamma_{Fe}) - \log(\gamma_O) \quad \text{Eq. 2}$$

a, b and ε_O^S were set equal to those from the second fit (reported in Table S-6) while T, x_S, x_{FeO} and x_{Fe} correspond to

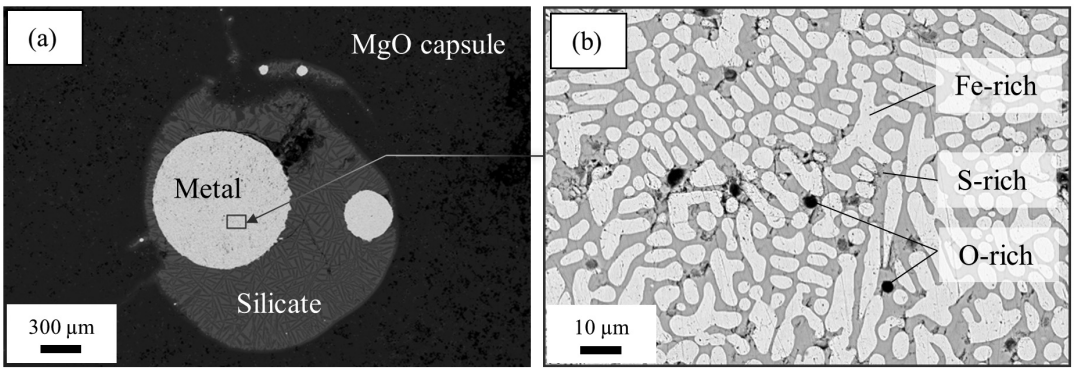

Figure 1 **(a)** BSE (backscattered electron) image of one of the recovered samples (ELMO 445, $P = 2$ GPa and $T = 1873$ K). The contrast is linked to changes in atomic number, with light areas corresponding to heavy (high-Z) phases (*e.g.*, iron) and dark phases to lighter (low-Z) material (*e.g.*, silicate). **(b)** BSE image of the metallic phase. The dendritic pattern results from the exsolution of two different metallic melts as the system cools during quench (the light-coloured phase is an iron-rich melt, and the darker phase is a sulfur-rich melt). The oxygen-rich blobs were lost while polishing and the observed dark spots correspond to their print in the structure.

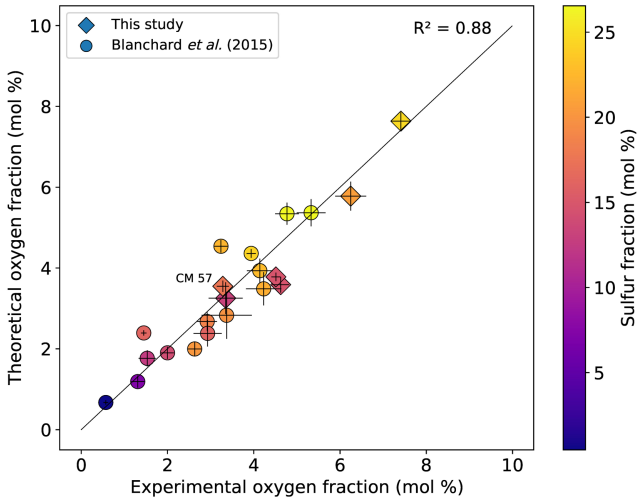

Figure 2 Predicted oxygen concentration (mol %) in the metallic phase *versus* measured oxygen concentration (mol %). Symbol colour is matched to the sulfur content (mol %) of each experiment, according to the colour bar to the right. The theoretical predictions (y-axis) fall close to the real values (x-axis) including CM 57 that equilibrated at a higher pressure (12 GPa). The vertical errors were set equal to the horizontal ones (1σ standard error) for simplification.

the experimental values. The results are plotted in Figure 2, and show an excellent agreement between our predictions and the data as the points do not scatter from the theoretical ideal 1:1 line ($R^2 = 0.88$), putting the model on robust grounds.

Core Composition Modelling

We incorporated our parametrisation of the oxygen-sulfur interaction in a multi-stage core formation model (Badro *et al.*, 2015) that was adapted for Mars (See Supplementary Information). The model tracks the oxygen and silicon concentrations in the core as well as the final pressure at the base of the magma ocean (output parameters) for a given sulfur content in the core, iron oxide fraction in the mantle and geotherm (input parameters). The outcome of our models is detailed in Table S-7 and further summarised in Figure 3 below where we plotted the oxygen concentration in the Martian core as a function of its sulfur content for a solidus (Fig. 3a) and a liquidus (Fig. 3b) magma ocean geotherm. The blue and red curves correspond to the computed oxygen fractions in the Martian core, either assuming an iron-rich (Sanloup *et al.*, 1999; Taylor, 2013) or an iron-poor (Yoshizaki and McDonough, 2020) Martian mantle. The range of oxygen concentrations in the core for a given mantle composition is therefore bracketed by these two curves for each mantle composition model.

As expected, the liquidus allows for dissolution of more oxygen than the solidus. Yet, this effect is of second order since the difference between the two is 0.4 wt. % O at most. The choice of mantle composition also influences the final results since the FeO-rich mantle of Taylor (2013) results in greater oxygen concentrations in the core and favours a shallow magma ocean, while the model of Yoshizaki and McDonough (2020) yields less oxygen in the core and requires a deeper magma ocean that can even reach the CMB for an S-poor core. We additionally observe that the Si content in the core remains negligible (≤0.07 wt. %) during the whole differentiation process (as seen in Fig. S-6f and further observed for all the simulations), confirming previous results by Gessmann *et al.* (2001), who found that Martian equilibrium conditions cannot dissolve a substantial amount of Si in the metal. Likewise, core formation modelling by Brennan *et al.* (2020) only gives a little fraction of Si in the Martian core, but also leads to less than 1 wt. % O in an S-rich core. This is a result of the fact that their modelling did not take into account O-S interaction during metal-silicate differentiation, thus severely underestimating the final amount of oxygen in Mars's core. Running our models with $\epsilon_O^S = 0$ (equivalent to no O-S interaction) gives a core with less than 0.6 wt. % O, consistent with their findings. This stresses the importance of taking into account all

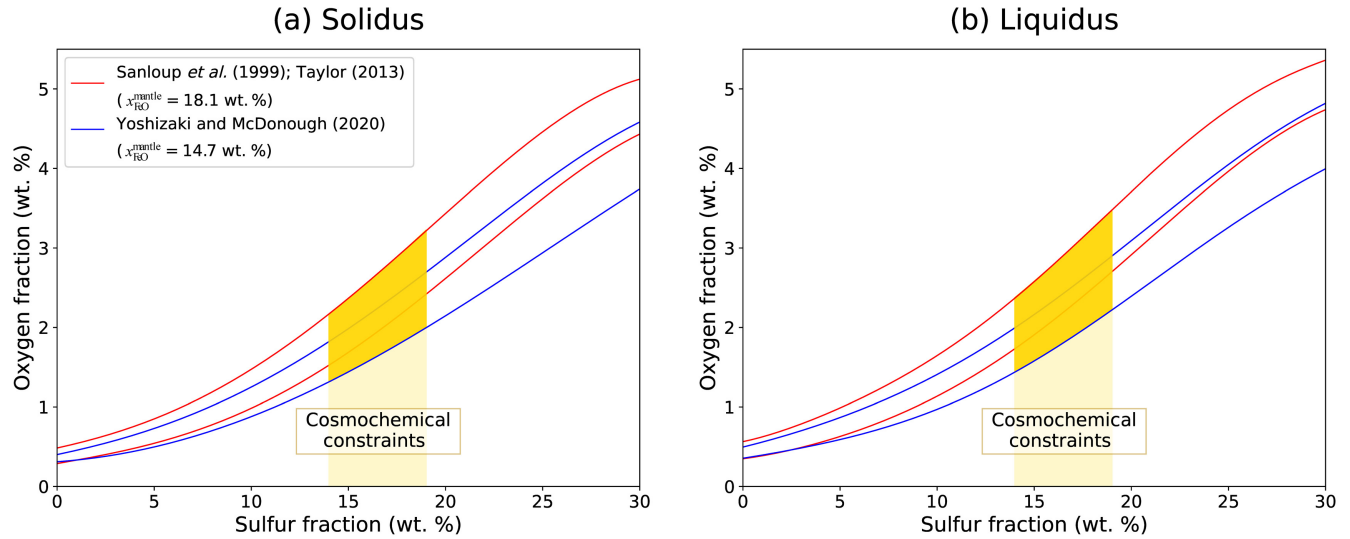

Figure 3 Predicted amount of oxygen in the Martian core for an FeO-rich (Sanloup *et al.*, 1999; Taylor, 2013) (red curves) and an FeO-poor mantle (Yoshizaki and McDonough, 2020) (blue curves). The curves were obtained by fitting the output data (Table S-7) with either a 4th order (solidus) or a 6th order (liquidus) polynomial (See Supplementary Information). For each of these mantle compositions, the associated amount of oxygen in the core is bracketed between a minimum and a maximum defined by the two curves of the same colour. They reflect the range of possible magma ocean depths at which the core can form. Both **(a)** solidus and **(b)** liquidus geotherms were tested. Cosmochemical constraints predict <14–19 wt. % S in the Martian core (Steenstra and van Westrenen, 2018; Brennan *et al.*, 2020) (yellow shaded area) that could lead up to 3.5 wt. % O in the core.

thermodynamic aspects of metal-silicate interactions when modelling systems that contain large amounts of light elements, such as Mars's core.

The maximum core density of Mars (6300 kg/m^3) necessitates on average 22–29 wt. % S (Figure S11-1 of Stähler *et al.*, 2021), if it is the sole light element. This exceeds the range (14–19 wt. % S) allowed by cosmochemical constraints (Steenstra and van Westrenen, 2018; Brennan *et al.*, 2020). Alternatively, a core with 19 wt. % S (consistent with cosmochemical constraints) would contain as much as 3.5 wt. % O (Fig. 3). Because 1 wt. % O has the same effect on density as 1.3 wt. % S (Stähler *et al.*, 2021), such a core would have the same density as a S-only core containing 23.6 wt. % S. As the Martian core is likely lighter than this, we see that an Fe–O–S core would still require a high fraction of S (>19 wt. %) that is non-permissible in cosmochemistry.

Conclusions

Our work predicts the possible dissolution of up to 3.5 wt. % O in the Martian core alongside 19 wt. % S that would fit within the upper core density estimate and be in agreement with cosmochemical constraints. While the dissolution of oxygen in the terrestrial core was driven by the very high pressures (~55 GPa) and high temperatures (3300–3400 K) that prevailed at the base of the magma ocean (Siebert *et al.*, 2012; Badro *et al.*, 2015; Fischer *et al.*, 2015), the amount of oxygen in the Martian core only results from its interaction with sulfur. This unavoidable concomitance of S and O in the Martian core should be taken into account in future Martian compositional models.

Acknowledgements

We thank two anonymous reviewers whose comments helped to substantially improve the paper. We thank Attilio Rivoldini for fruitful discussions as well as Kurt Leinenweber, Julien Siebert, and Edith Kubik for the experimental and analytical help. We also thank Pierre-Olivier Foucault for designing the graphical abstract. We acknowledge the financial support of the UnivEarthS Labex program at Université Paris Cité (ANR-10-LABX-0023 and ANR-11-IDEX-0005-02), and IdEx Université Paris Cité (ANR-18-IDEX-0001). This work has received funding from the European Research Council (ERC) under the European Union's Horizon 2020 research and innovation programme (grant agreement no. 101019965— SEPtiM). Parts of this work were supported by IPGP multidisciplinary program PARI, and by Paris–IdF region SESAME Grant no. 12015908.

Editor: Anat Shahar

Additional Information

Supplementary Information accompanies this letter at https://www.geochemicalperspectivesletters.org/article2216.

Cite this letter as: Gendre, H., Badro, J., Wehr, N., Borensztajn, S. (2022) Martian core composition from experimental high-pressure metal-silicate phase equilibria. *Geochem. Persp. Let.* 21, 42–46. https://doi.org/10.7185/geochemlet.2216

References

Badro, J., Brodholt, J.P., Piet, H., Siebert, J., Ryerson, F.J. (2015) Core formation and core composition from coupled geochemical and geophysical constraints. *Proceedings of the National Academy of Sciences* 112, 12310–12314. https://doi.org/10.1073/pnas.1505672112

Bertka, C.M., Fei, Y. (1998) Implications of Mars Pathfinder Data for the Accretion History of the Terrestrial Planets. *Science* 281, 1838–1840. https://doi.org/10.1126/science.281.5384.1838

Blanchard, I., Badro, J., Siebert, J., Ryerson, F.J. (2015) Composition of the core from gallium metal–silicate partitioning experiments. *Earth and Planetary Science Letters* 427, 191–201. https://doi.org/10.1016/j.epsl.2015.06.063

Brennan, M.C., Fischer, R.A., Irving, J.C.E. (2020) Core formation and geophysical properties of Mars. *Earth and Planetary Science Letters* 530, 115923. https://doi.org/10.1016/j.epsl.2019.115923

Dreibus, G., Wanke, H. (1985) Mars, a volatile-rich planet. *Meteoritics* 20, 367–381.

Fei, Y., Prewitt, C.T., Mao, H.-K., Bertka, C.M. (1995) Structure and Density of FeS at High Pressure and High Temperature and the Internal Structure of Mars. *Science* 268, 1892–1894. https://doi.org/10.1126/science.268.5219.1892

Fischer, R.A., Nakajima, Y., Campbell, A.J., Frost, D.J., Harries, D., Langenhorst, F., Miyajima, N., Pollok, K., Rubie, D.C. (2015) High pressure metal–silicate partitioning of Ni, Co, V, Cr, Si, and O. *Geochimica et Cosmochimica Acta* 167, 177–194. https://doi.org/10.1016/j.gca.2015.06.026

Gessmann, C.K., Wood, B., Rubie, D.C., Kilburn, M.R. (2001) Solubility of silicon in liquid metal at high pressure: Implications for the composition of the Earth's core. *Earth and Planetary Science Letters* 184, 367–376. https://doi.org/10.1016/S0012-821X(00)00325-3

Khan, A., Liebske, C., Rozel, A., Rivoldini, A., Nimmo, F., Connolly, J.A.D., Plesa, A.-C., Giardini, D. (2018) A Geophysical Perspective on the Bulk Composition of Mars. *Journal of Geophysical Research: Planets* 123, 575–611. https://doi.org/10.1002/2017JE005371

Lodders, K., Fegley Jr., B. (1997) An Oxygen Isotope Model for the Composition of Mars. *Icarus* 126, 373–394. https://doi.org/10.1006/icar.1996.5653

McSween Jr., H.Y. (1994) What we have learned about Mars from SNC meteorites. *Meteoritics* 29, 757–779. https://doi.org/10.1111/j.1945-5100.1994.tb01092.x

Morard, G., Sanloup, C., Fiquet, G., Mezouar, M., Rey, N., Poloni, R., Beck, P. (2007) Structure of eutectic Fe–FeS melts to pressures up to 17 GPa: Implications for planetary cores. *Earth and Planetary Science Letters* 263, 128–139. https://doi.org/10.1016/j.epsl.2007.09.009

Morard, G., Bouchet, J., Rivoldini, A., Antonangeli, D., Roberge, M., Boulard, E., Denoeud, A., Mezouar, M. (2018) Liquid properties in the Fe-FeS system under moderate pressure: Tool box to model small planetary cores. *American Mineralogist* 103, 1770–1779. https://doi.org/10.2138/am-2018-6405

Morgan, J.W., Anders, E. (1979) Chemical composition of Mars. *Geochimica et Cosmochimica Acta* 43, 1601–1610. https://doi.org/10.1016/0016-7037(79)90180-7

Ohtani, E., Ringwood, A.E., Hibberson, W. (1984) Composition of the core, II. Effect of high pressure on solubility of FeO in molten iron. *Earth and Planetary Science Letters* 71, 94–103. https://doi.org/10.1016/0012-821X(84)90055-4

Ricolleau, A., Fei, Y., Corgne, A., Siebert, J., Badro, J. (2011) Oxygen and silicon contents of Earth's core from high pressure metal–silicate partitioning experiments. *Earth and Planetary Science Letters* 310, 409–421. https://doi.org/10.1016/j.epsl.2011.08.004

Righter, K. (2017) The Martian Meteorite Compendium. https://curator.jsc.nasa.gov/antmet/mmc/

Rivoldini, A., Van Hoolst, T., Verhoeven, O., Mocquet, A., Dehant, V. (2011) Geodesy constraints on the interior structure and composition of Mars. *Icarus* 213, 451–472. https://doi.org/10.1016/j.icarus.2011.03.024

Sanloup, C., Jambon, A., Gillet, P. (1999) A simple chondritic model of Mars. *Physics of the Earth and Planetary Interiors* 112, 43–54. https://doi.org/10.1016/S0031-9201(98)00175-7

Siebert, J., Badro, J., Antonangeli, D., Ryerson, F.J. (2012). Metal–silicate partitioning of Ni and Co in a deep magma ocean. *Earth and Planetary Science Letters* 321–322, 189–197. https://doi.org/10.1016/j.epsl.2012.01.013

Siebert, J., Badro, J., Antonangeli, D., Ryerson, F.J. (2013) Terrestrial Accretion Under Oxidizing Conditions. *Science* 339, 1194–1197. https://doi.org/10.1126/science.1227923

Stähler, S.C., Khan, A., Banerdt, W.B., Lognonné, P., Giardini, D., Ceylan, S., Drilleau, M., Duran, A.C., Garcia, R.F., Huang, Q., Kim, D., Lekic, V., Samuel, H., Schimmel, M., Schmerr, N., Sollberger, D., Stutzmann, E., Xu, Z., Antonangeli, D., Charalambous, C., Davis, P.M., Irving, J.C.E., Kawamura, T., Knapmeyer, M., Maguire, R., Marusiak, A.G., Panning, M.P., Perrin, C., Plesa, A.-C., Rivoldini, A., Schmelzbach, C., Zenhäusern, G., Beucler, E., Clinton, J., Dahmen, N., van Driel, M., Gudkova, T., Horleston, A., Pike, W.T., Plasman, M., Smrekar, S. (2021) Seismic detection of the martian core. *Science* 373, 443–448. https://doi.org/10.1126/science.abi7730

Steelmaking Data Sourcebook (1988) The Japan Society for the Promotion of Science: The 19th Committee on Steelmaking. Gordon and Breach Science Publishers, New York.

Steenstra, E.S., van Westrenen, W. (2018) A synthesis of geochemical constraints on the inventory of light elements in the core of Mars. *Icarus* 315, 69–78. https://doi.org/10.1016/j.icarus.2018.06.023

Taylor, G.J. (2013) The bulk composition of Mars. *Geochemistry* 73, 401–420. https://doi.org/10.1016/j.chemer.2013.09.006

Terasaki, H., Rivoldini, A., Shimoyama, Y., Nishida, K., Urakawa, S., Maki, M., Kurokawa, F., Takubo, Y., Shibazaki, Y., Sakamaki, T., Machida, A., Higo, Y., Uesugi, K., Takeuchi, A., Watanuki, T., Kondo, T. (2019) Pressure and Composition Effects on Sound Velocity and Density of Core-Forming Liquids: Implication to Core Compositions of Terrestrial Planets. *Journal of Geophysical Research: Planets* 124, 2272–2293. https://doi.org/10.1029/2019JE005936

Tsuno, K., Frost, D.J., Rubie, D.C. (2011) The effects of nickel and sulphur on the core–mantle partitioning of oxygen in Earth and Mars. *Physics of the Earth and Planetary Interiors* 185, 1–12. https://doi.org/10.1016/j.pepi.2010.11.009

Yoshizaki, T., McDonough, W.F. (2020) The composition of Mars. *Geochimica et Cosmochimica Acta* 273, 137–162. https://doi.org/10.1016/j.gca.2020.01.011

Zharkov, V.N., Gudkova, T.V. (2005) Construction of Martian Interior Model. *Solar System Research* 39, 343–373. https://doi.org/10.1007/s11208-005-0049-7